PROCEEDINGS OF SCIENCE

Heavy flavour production in ATLAS: Charmonium production in $p-p$ at 13 TeV and in $Pb-Pb$ collisions. Associated charmonium and vector bosons production.

Brad Abbott[*†]
University of Oklahoma
E-mail: abbott@ou.edu

Five results are presented for charmonium production in pp, $p-Pb$ and $Pb-Pb$ collisions. Measurements of per-event yields, nuclear modification factors and non-prompt fractions are presented for J/ψ and $\psi(2S)$ in $Pb+Pb$ collisions at $\sqrt{S_{NN}}$ = 5.02 TeV and pp collisions at $\sqrt{s}$=5.02 TeV. The modification of the production of J/ψ, $\psi(2S)$, and $\Upsilon(1S)$, $\Upsilon(2S)$, and $\Upsilon(3S)$ in $p+Pb$ collisions relative to their production in pp collision is measured at a center of mass energy per nuclean pair of 5.02 TeV. The elliptic flow of both prompt and non prompt J/ψ is measured in $Pb+Pb$ collisions at $\sqrt{S_{NN}}$ = 5.02 TeV. Measurements of prompt and non-prompt J/ψ and $\psi(2S)$ mesons with p_T between 60-360 GeV is reported at $\sqrt{s}$= 13 TeV in pp collisions. A measurement of the production of a prompt J/ψ in association with a W is presented at $\sqrt{s}$=8 TeV in pp collisions.

18th International Conference on B-Physics at Frontier Machines - Beauty2019 -
29 September / 4 October, 2019
Ljubljana, Slovenia

[*]Speaker.
[†]For the ATLAS Collaboration

PoS(Beauty2019)023

1. Charmonium Production in $Pb-Pb$

The modification of prompt J/ψ production is not expected to be similar to non-prompt J/ψ production since different mechanisms contribute to the final states. Simultaneous measurements of both prompt and non-prompt charmonia are critical for understanding the mechanisms of charmonium suppression in heavy-ion collisions.

We report prompt and non-prompt per-event yields, non-prompt fraction and the nuclear modification factor, R_{AA}, of the J/ψ and $\psi(2S)$ as a function of P_T, rapidity and centrality. The measurements are made in the dimuon decay channel in $Pb+Pb$ collisions at $\sqrt{S_{NN}}$ = 5.02 TeV and in pp collisions at $\sqrt{s}$=5.02 TeV [1].

The pseudo-proper decay time

$$\tau = \frac{L_{xy} m_{\mu\mu}}{p_T^{\mu\mu}}$$

is used to discriminate between prompt and non-prompt production, where $m_{\mu\mu}$ and $p_T^{\mu\mu}$ are the reconstructed mass and transverse momentum of the dimuon system, respectively and L_{xy} is the distance between the position of the reconstructed dimuon vertex and the primary vertex projected into the transverse plane. All events are weighted to take into account the acceptance, reconstruction efficiency and trigger efficiency. A two-dimensional unbinned maximum-likelihood fit to the dimuon invariant mass and pseudo-proper time of weighted events is used to extract the prompt and non-prompt charmonium components.

The suppression of charmonium states is quantified by the nuclear modification factor which is defined for a given centrality as

$$R_{AA} = \frac{N_{AA}}{\langle T_{AA} \rangle \times \sigma_{pp}}$$

where N_{AA} is the per-event yield of charmonium states, $\langle T_{AA} \rangle$ is the mean nuclear thickness function and σ_{pp} is the cross section for the production of the corresponding charmonium state in pp collisions at the same energy.

Centrality of $Pb+Pb$ collisions is characterized by the sum of the transverse energy in the forward calorimeter and describes the degree of geometrical overlap of the two colliding nuclei in the plane perpendicular to the beam.

Figure 1 shows the nuclear modification factor as a function of p_T for prompt J/ψ and non-prompt J/ψ for different centrality bins. The production of J/ψ is strongly suppressed in central $Pb-Pb$ collisions and the suppression for non-prompt J/ψ is consistent with being independent of p_T.

Figure 2 (left) shows a measurement of the prompt and non-prompt J/ψ nuclear modification factor as a function of p_T. A small increase is seen and is similar in shape to that observed for charged particles. Figure 2 (right) shows a comparison of R_{AA} for several theoretical models to prompt J/ψ production. The measurements are consistent with the color screening and parton-energy loss models. The suppression is a sign that the hot dense medium has a strong influence on particle production processes.

Figure 3 (top) shows the nuclear modification factor as a function of N_{part} for production of prompt and non-prompt J/ψ which shows that both prompt and non-prompt J/ψ have similar behavior. This is not expected since non-prompt production is dominated by b-decays that extend

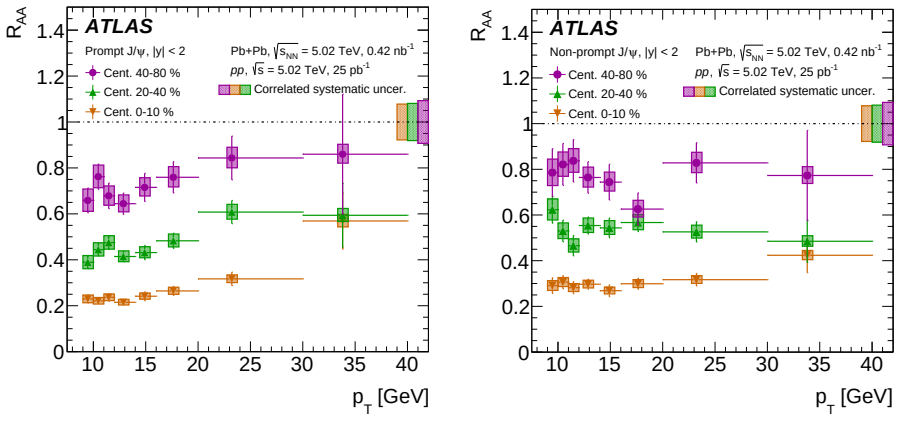

Figure 1: The nuclear modification factor as a function of p_T for prompt J/ψ (left) and non-prompt J/ψ (right) for different centrality bins [1] .

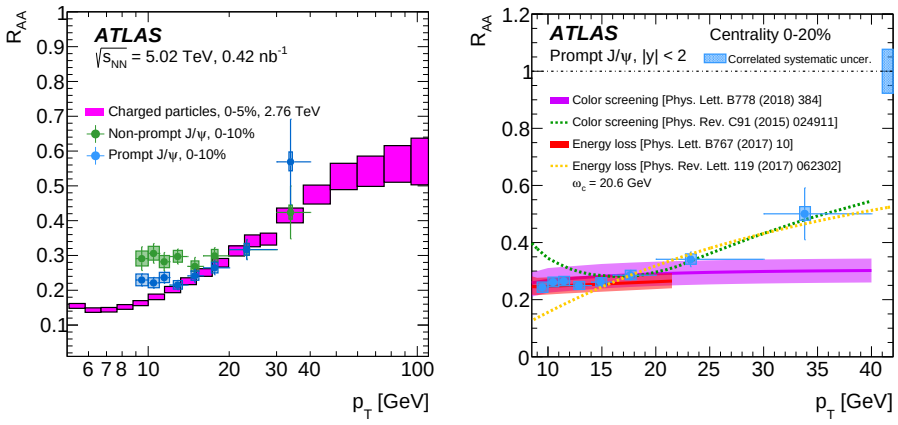

Figure 2: Comparison of the prompt and non-prompt J/ψ nuclear modification factor to that of charged particles (left). Comparison of R_{AA} for different theoretical models to prompt J/ψ production (right) [1].

outside the medium while prompt production happens primarily within the medium. The double ratio of $\psi(2S)$ production to J/ψ production is shown in Figure 3 (bottom). These results are consistent with the interpretation that the tighter bound J/ψ survives in the hot and dense medium with higher probability than the more loosely bound $\psi(2S)$. The non-prompt double ratio is consistent with unity suggesting both mesons originate from b-quarks. For further details about these results see [1].

2. Quarkonium Production in pp and pPb

The study of heavy quarkonium bound states in heavy-ion collisions may be used as a probe to study the deconfined quark-gluon plasma (QGP) created in nucleus-nucleus collisions. To understand quarkonium yields in nucleus-nucleus collision, one must disentangle the effects due to

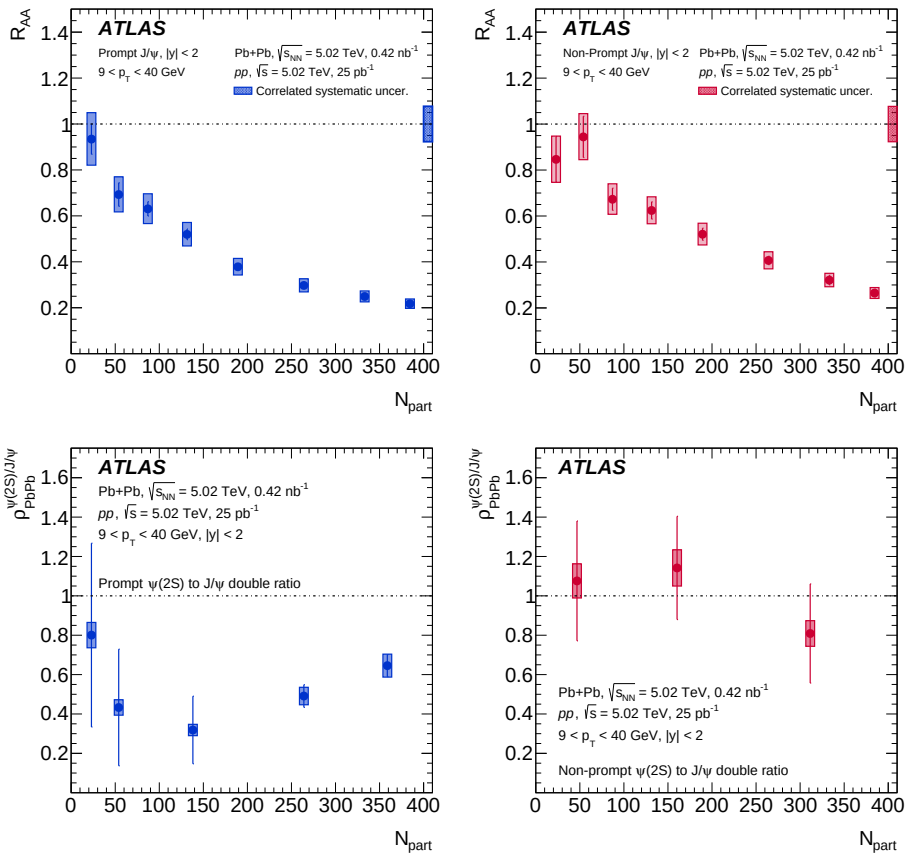

Figure 3: R_{AA} as a function of the number of participants for prompt J/ψ (top left) and non-prompt J/ψ (top right). The $\psi(2S)$ to J/ψ double ratio as a function of the number of participants for prompt meson production (bottom left) and non-prompt meson production (bottom right) [1].

the interactions between quarkonium and the QGP medium and those from cold nuclear matter. By studying the suppression of quarkonium, the effects of cold nuclear matter may be determined.

The modification of quarkonium production in $p+Pb$ collision relative to pp collisions can be described by the nuclear modification factor

$$R_{pPb} = \frac{1}{208}\frac{\sigma^{O(nS)}_{p+Pb}}{\sigma^{O(nS)}_{pp}}$$

where $O(nS)$ represents one of the measured quarkonium states J/ψ, $\psi(2S)$, $\Upsilon(1S)$, $\Upsilon(2S)$ and $\Upsilon(3S)$.

The dataset consists of $p+Pb$ collisions and pp collisions both recorded at a center of mass energy of 5.02 TeV per nucleon pair [2]. The measurements are made in the dimuon decay channel. All events are weighted to take into account the acceptance, reconstruction efficiency and trigger efficiency. A two-dimensional unbinned maximum-likelihood fit to the dimuon invariant mass and pseudo-proper time of weighted events is used to extract the prompt and non-prompt charmonium

components. The bottomonium yields are extracted using an unbinned maximum likelihood fit of the weighted invariant mass distribution.

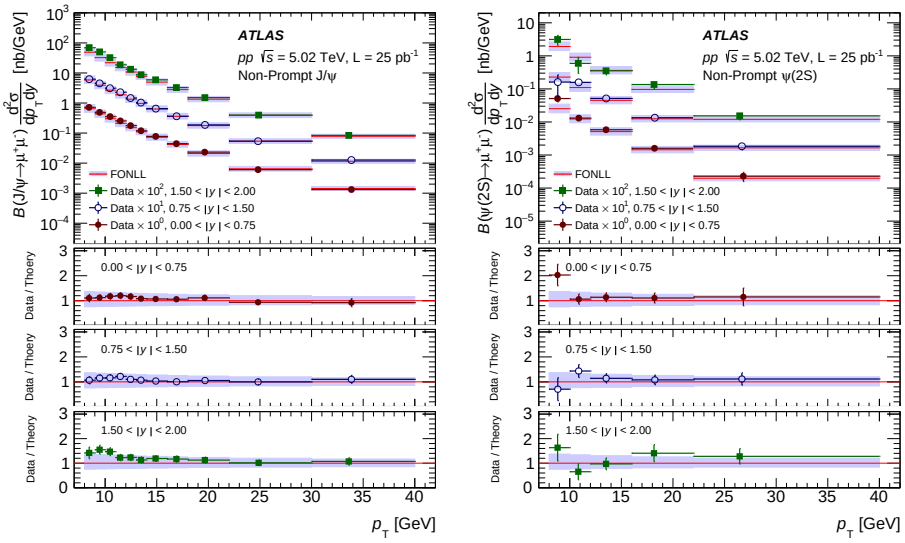

Figure 4: Differential non-prompt production cross section times the dimuon branching fraction for J/ψ(right) and $\psi(2S)$ (left) as a function of p_T. FONLL theory predictions are also shown [2].

Figure 4 shows the differential non-prompt production cross section times the dimuon branching fraction for J/ψ and $\psi(2S)$ as a function of p_T compared to FONLL [3] predictions. Good agreement is observed between the non-prompt data and FONLL.

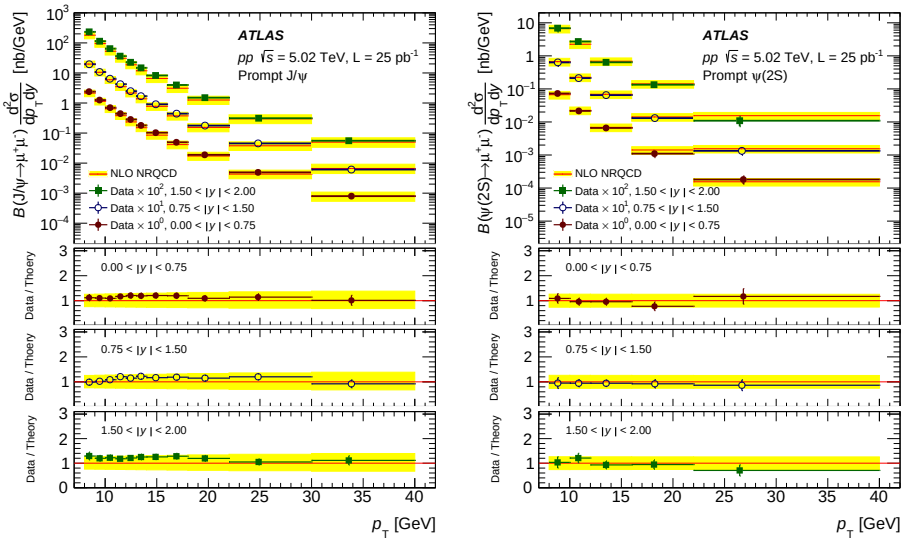

Figure 5: Differential prompt production cross section times the dimuon branching fraction for J/ψ(right) and $\psi(2S)$ (left) as a function of p_T. Predictions from NRQCD are also shown [2].

Figure 5 shows the differential prompt production cross section times the dimuon branching fraction for J/ψ and $\psi(2S)$ as a function of p_T compared to NRQCD [4] predictions. The theory

predictions are based on long-distance matrix elements from [5, 6]. Good agreement is observed between the prompt data and the NRQCD predictions.

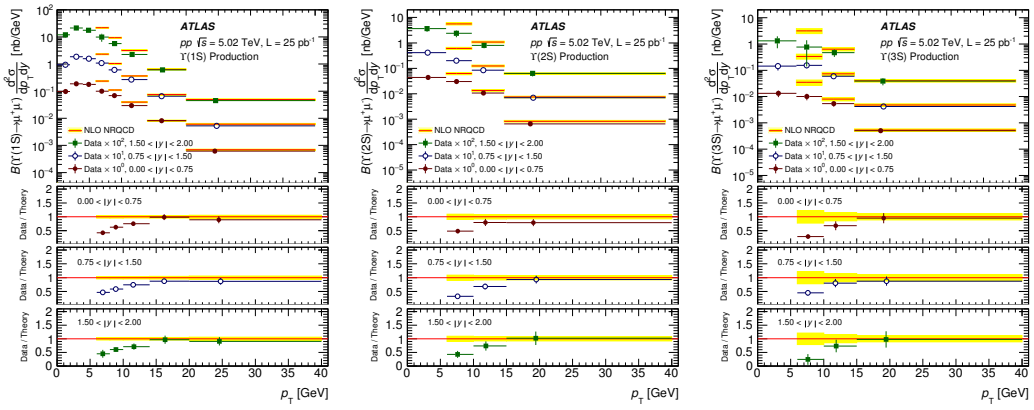

Figure 6: Differential prompt production cross section times the dimuon branching fraction for $\Upsilon(1S)$ (left), $\Upsilon(2S)$ (middle) and $\Upsilon(3S)$ (right) as a function of p_T. NRQCD theory predictions are also shown [2].

Figure 6 shows the differential prompt production cross section times the dimuon branching fraction for $\Upsilon(1S)$, $\Upsilon(2S)$ and $\Upsilon(3S)$ as a function of p_T compared to NRQCD predictions. Good agreement is observed between data and NRQCD for p_T> 15 GeV.

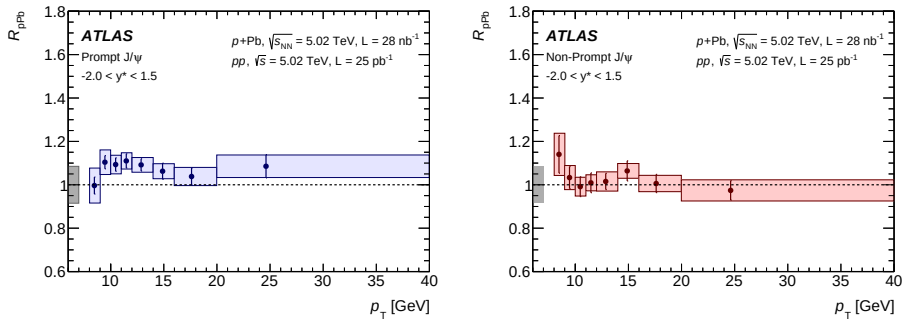

Figure 7: The nuclear modification factor for prompt J/ψ (left) and non-prompt J/ψ (right) as a function of p_T [2].

Figure 7 shows the nuclear modification factor for prompt and non-prompt J/ψ as a function of p_T while Figure 8 shows the nuclear modification factor for $\Upsilon(1S)$ as a function of p_T and center-of-mass rapidity y^*.

Prompt and non-prompt J/ψ are consistent with unity across the measured p_T range but $\Upsilon(1S)$ shows a significant discrepancy with unity at low p_T. The observed suppression of $\Upsilon(1S)$ may come from the reduction of hard scattering cross sections due to strong nPDF shadowing at smaller Bjorken-x. For further details about these results see [2].

3. J/ψ Elliptic Flow in $Pb-Pb$

Studying prompt vs non-prompt J/ψ mesons probes the flavor dependence of the hot dense

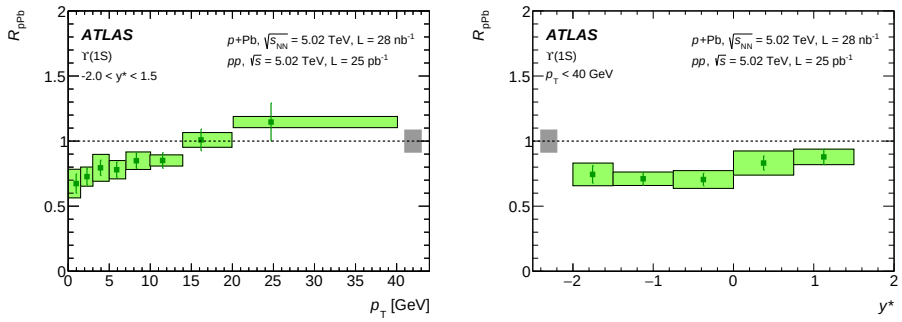

Figure 8: The nuclear modification factor for $\Upsilon(1S)$ as a function of p_T (left) and center-of-mass rapidity y^* (right) [2].

plasma produced in $Pb-Pb$ collisions. In non-central collisions the overlap region of the Pb ions has an elliptic shape and the particle yield is affected by this distribution. This leads to an azimuthal anisotropy relative to the reaction plane that can be characterized by a Fourier expansion:

$$\frac{dN}{d\phi} \propto 1 + \Sigma_{n=1}^{\infty} 2v_n \cos[n(\phi - \Psi_n)],$$

where ϕ is the azimuthal angle relative to the detector frame of reference, and Ψ_n is the n-th harmonic of the event-plane angle. The coefficient v_2 is called the elliptic flow and its size measures the yield relative to the initial elliptical matter distribution.

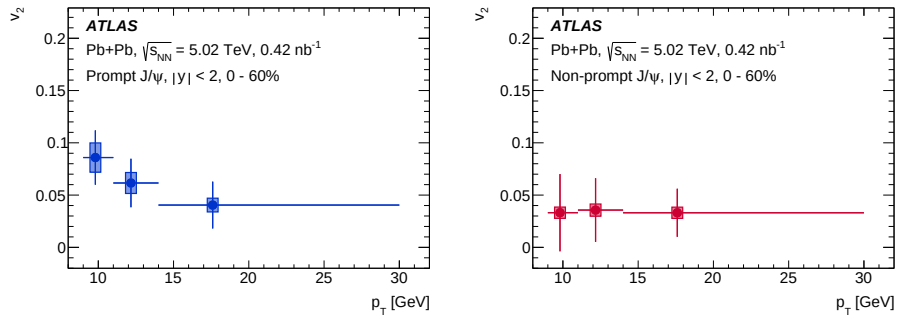

Figure 9: v_2 for prompt (left) and non-prompt (right) J/ψ mesons as a function of p_T [7].

The data is from $Pb+Pb$ collisions at $\sqrt{s_{NN}}$ = 5.02 TeV [7]. The measurements are made in the dimuon decay channel. All events are weighted to take into account the acceptance, reconstruction efficiency and trigger efficiency. A two-dimensional unbinned maximum-likelihood fit to the dimuon invariant mass and pseudo-proper time of weighted events is used to extract the prompt and non-prompt charmonium components. The J/ψ v_2 is measured using the event-plane method [8].

Figure 9 shows v_2 for both prompt and non-prompt J/ψ mesons as a function of p_T. For non-prompt J/ψ, v_2 is consistent with being independent of p_T while for prompt J/ψ, v_2 decreases

with increasing p_T. At high p_T, similar v_2 for prompt and non-prompt J/ψ suggest a similar suppression mechanism at high p_T.

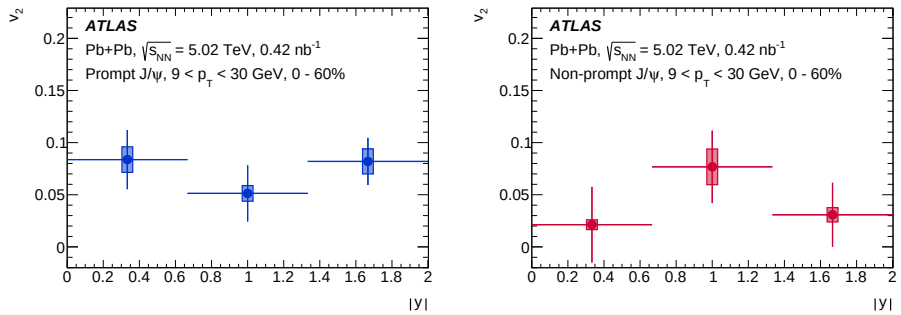

Figure 10: v_2 for prompt (left) and non-prompt (right) J/ψ mesons as a function of rapidity [7].

Figure 10 shows v_2 for prompt and non-prompt J/ψ mesons as a function of rapidity. No significant rapidity dependence is seen for either prompt and non-prompt J/ψ mesons. For further details about these results see [7].

4. Charmonium High p_T production cross sections in pp collisions at 13 TeV

Charmonium production provides insight into QCD near the boundary of perturbative and non-perturbative regimes. Previous ATLAS measurements of cross sections primarily used dimuon triggers with low thresholds which limited the measurement to p_T<100 GeV. Measuring high p_T production of quarkonium states is important because high p_T behavior may help discriminate between various theoretical models. By using single muon triggers and the full Run 2 dataset, measurements at high p_T (60-360 GeV) are possible, significantly expanding the range.

The dataset consists of 139 fb^{-1} of data collected at $\sqrt{s}$=13 TeV [9]. The measurements are made in the dimuon decay channel. All events are weighted to take into account the acceptance, reconstruction efficiency and trigger efficiency. A two-dimensional unbinned maximum-likelihood fit to the dimuon invariant mass and pseudo-proper time of weighted events is used to extract the prompt and non-prompt charmonium components.

Figure 11 shows the differential cross sections of prompt and non-prompt production for both J/ψ and $\psi(2S)$. Figure 12 shows the non-prompt production fraction for both J/ψ and $\psi(2S)$ after all correction have been applied. Figure 13 shows the ratio of $\psi(2S)$ production with respect to J/ψ for both prompt and non-prompt production mechanisms after all corrections have been applied. Figure 14 shows the ratio of the FONLL [3, 10] prediction to the measured differential cross sections for both non-prompt J/ψ and $\psi(2S)$ mesons.

The results show similar p_T dependence for both prompt and non-prompt differential distributions. The non-prompt fractions are nearly constant as a function of p_T for both J/ψ and $\psi(2S)$ The FONLL predictions are consistent with data in the lower p_T range for non-prompt production but exceed the experimental results at larger p_T. For further details about these results see [9].

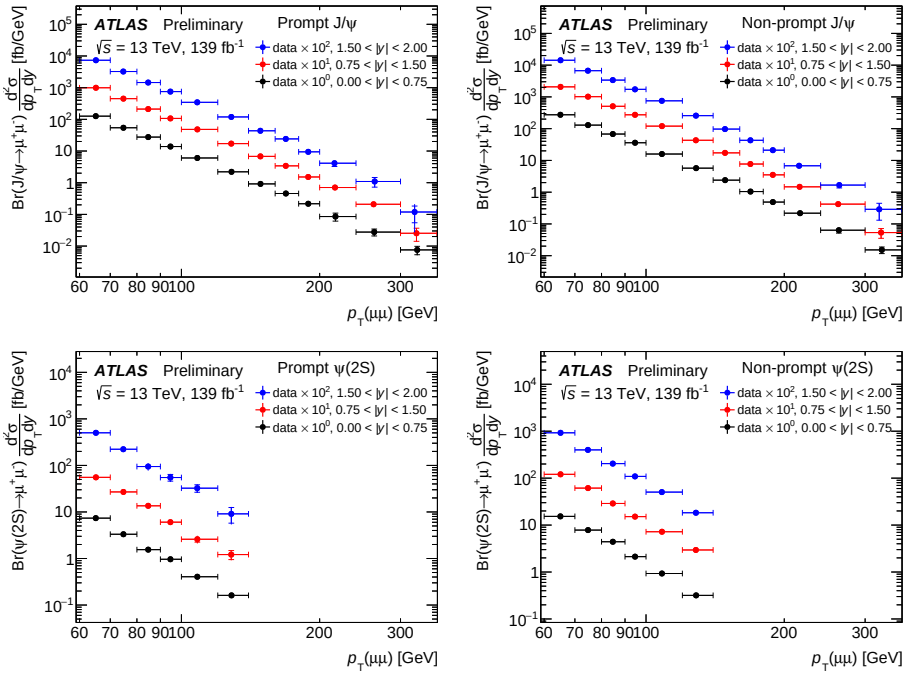

Figure 11: Differential cross sections of prompt and non-prompt production of J/ψ mesons (top) and $\psi(2S)$ mesons (bottom) [9].

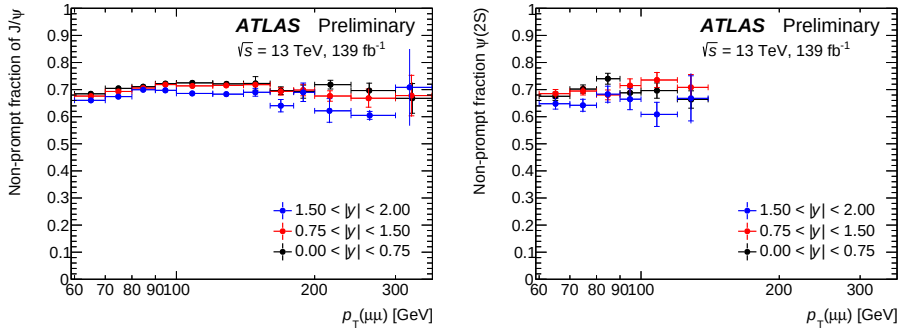

Figure 12: Non-prompt production fraction for J/ψ (left) and $\psi(2S)$ (right) after all corrections have been applied [9].

5. J/ψ production in association with a W boson in pp collisions at 8 TeV

The production mechanism of charmonium in hadronic collisions is not fully understood with the relative contribution of the color singlet to the color octet being unknown. Requiring an associated object, such as a W boson, filters the possible color singlet/color octet diagrams. In addition, the contributions of double parton scattering (DPS) versus single parton scattering (SPS) is unknown and $J/\psi + W$ can probe the relative contributions by measuring $\Delta\phi$ between the two particles.

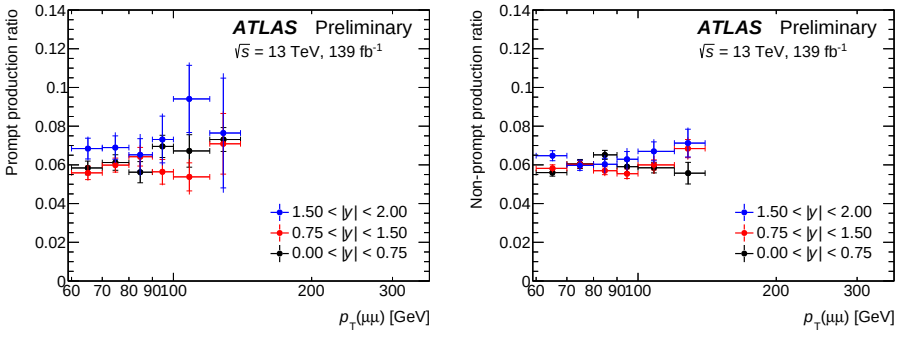

Figure 13: Ratio of $\psi(2S)$ production with respect to J/ψ for prompt (left) and non-prompt (right) production mechanisms after all corrections have been applied [9].

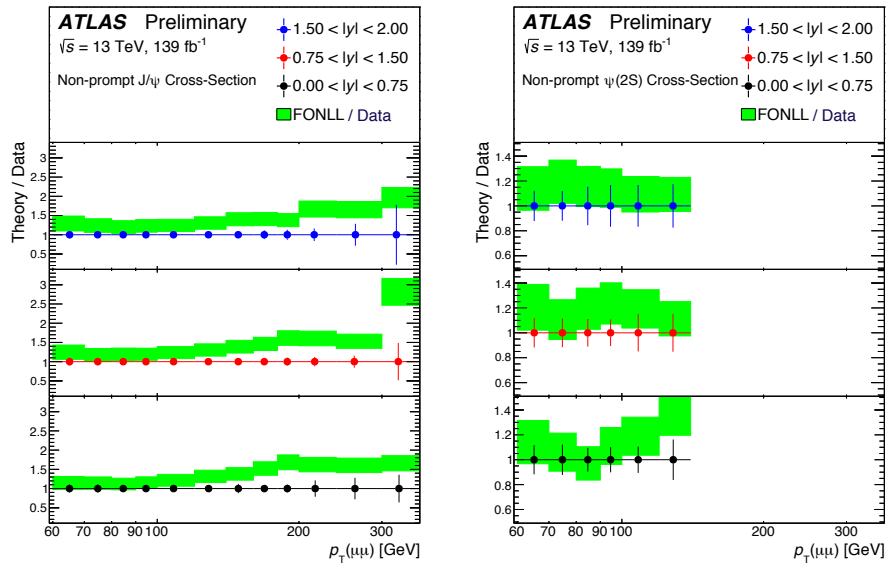

Figure 14: Ratio of the FONLL prediction to the measured differential cross sections for non-prompt J/ψ (left) and $\psi(2S)$ (right) mesons [9].

The dataset consists of 20.3 fb^{-1} of data collected at $\sqrt{s}$=8 TeV [11]. Events were selected using a non-prescaled single muon trigger. An inclusive W sample is defined by applying the selection shown in Table 1.

If an event has two muons which satisfy a J/ψ muon criteria, this defines the associated $J/\psi+W$ sample. All events in the associated sample are weighted to take into account the acceptance and reconstruction efficiency of the muons from the J/ψ. A two-dimensional unbinned maximum-likelihood fit to the dimuon invariant mass and pseudo-proper time of weighted events is used to extract the prompt charmonium components. After the fit is performed, the sPlot tool [12] is used to extract per-event weights which allows other signal distributions such as the azimuthal opening

Table 1: Selection criteria for the inclusive W sample, where μ is the muon from the W boson decay [11].

W boson selection
At least one isolated muon that originates < 1 mm from primary vertex along z-axis
p_{T} (trigger muon) $> 25\,\mathrm{GeV}$
$\lvert\eta^{\mu}\rvert < 2.4$
Missing transverse momentum $> 20\,\mathrm{GeV}$
$m_{\mathrm{T}}(W) > 40\,\mathrm{GeV}$
$\lvert d_0\rvert/\sigma_{d_0} < 3$

$\Delta\phi(J/\psi, W)$ to be generated.

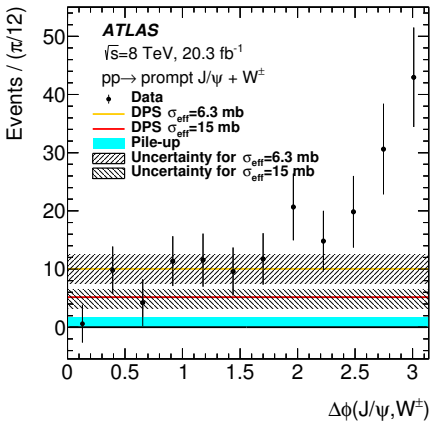

Figure 15: The sPlot-weighted opening angle $\Delta\phi(J/\psi, W)$ for prompt $J/\psi + W$ candidates [11].

Figure 15 shows the sPlot-weighted opening angle $\Delta\phi(J/\psi, W)$ for prompt $J/\psi + W$ candidates. Based on the assumptions that the two hard scatters are uncorrelated, the probability that a J/ψ is produced by a second hard process in an event containing a $W^{\pm}$ boson is given by

$$P^{ij}_{J/\psi|W} = \frac{\sigma^{ij}_{J/\psi}}{\sigma_{\mathrm{eff}}},$$

where $\sigma^{ij}_{J/\psi}$ is the cross-section for J/ψ production in the appropriate p_{T} (i) and rapidity (j) interval and σ_{eff} is the effective transverse overlap area of the interacting partons. Since σ_{eff} may not be process-independent, two different values are considered. Both choices of σ_{eff} are consistent with the data at low $\Delta\phi$. The data is consistent with contributions from both SPS and DPS processes.

The fully corrected inclusive production cross-section ratio, in which the J/ψ acceptance and the unknown J/ψ spin-alignment are taken into account, is given by

$$R^{\mathrm{incl}}_{J/\psi} = \frac{\sigma_{\mathrm{incl}}(pp \to J/\psi + W)}{\sigma(pp \to W)} \cdot \mathscr{B}(J/\psi \to \mu\mu) = \frac{1}{N(W)} \sum_{p_{\mathrm{T}}\ \mathrm{bins}} [N^{\mathrm{eff+acc}}(J/\psi + W) - N_{\mathrm{pile\text{-}up}}],$$

where $N^{\text{eff+acc}}(J/\psi+W)$ is the background subtracted yield of prompt $J/\psi+W$ events after J/ψ acceptance corrections and efficiency corrections for the J/ψ decay muons, and $N_{\text{pile-up}}$ is the expected number of pile-up events in the full range of J/ψ decay phase space. The result is

$$R^{\text{incl}}_{J/\psi} = (5.3 \pm 0.7 \pm 0.8^{+1.5}_{-0.7}) \times 10^{-6},$$

where the first uncertainty is statistical, the second systematic and the third is from the spin-alignment scenario.

Additional measurements are made by subtracting the estimated DPS contribution in each rapidity and p_{T} interval from the inclusive cross-section ratio,

$$R^{\text{DPSsub}}_{J/\psi} = (3.6 \pm 0.7^{+1.1\ +1.5}_{-1.0\ -0.7}) \times 10^{-6}, \ [\sigma_{\text{eff}} = 15^{+5.8}_{-4.2} \text{ mb}]$$

and

$$R^{\text{DPSsub}}_{J/\psi} = (1.3 \pm 0.7 \pm 1.5^{+1.5}_{-0.7}) \times 10^{-6}, \ [\sigma_{\text{eff}} = 6.3 \pm 1.9 \text{ mb}]$$

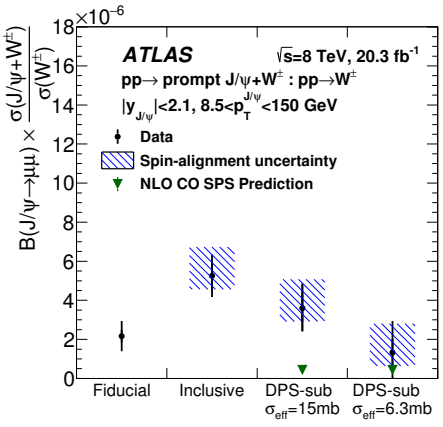

Figure 16: Production cross section ratios for the measurement in the fiducial volume (bin 1), the ratio corrected for acceptance effects (bin 2) and the ratio corrected for double parton scattering for two different choices of σ_{eff}. (bins 3,4). The data in bins 3 and 4 are compared to a NLO CO SPS prediction [11].

Figures 16 and 17 show the production cross section ratio and differential cross section ratio for two different choices of σ_{eff} compared to a NLO CO SPS prediction [13, 14]. A smaller value of σ_{eff} is preferred however neither value of σ_{eff} can describe the $p_T^{J/\Psi}$ dependence. For further details about these results see [11].

References

[1] ATLAS Collaboration, "Prompt and non-prompt J/ψ and $\psi(2S)$ suppression at high transverse momentum in 5.02 TeV $Pb+Pb$ collisions with the ATLAS experiment", Eur. Phys J. C78 (2018) 762

[2] ATLAS Collaboration, "Measurement of quarkonium production in proton-lead and proton-proton collisions at 5.02 TeV with the ATLAS detector", Eur. Phys J. C78 (2018) 171

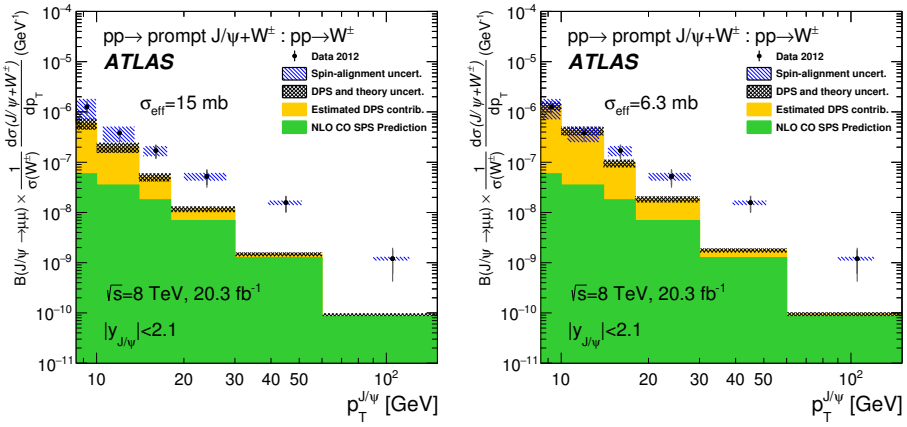

Figure 17: The inclusive differential cross-section ratio compared to theory in six $p_T^{J/\psi}$ regions for σ_{eff}=15 mb (left) and σ_{eff}=6.3 mb (right) [11].

[3] M. Cacciari et al. "Theoretical predictions for charm and bottom production at the LHC", JHEP **10** (2012) 137.

[4] H. Han et al., "$\Upsilon(nS)$ and $\chi_b(nP)$ production at hadron colliders in nonrelativistic QCD", Phys. Rev. D **94** (2016) 014028

[5] Y. Ma, K. Wang and K. Chao. "$J/\psi(\psi')$ Production at the Tevatron and LHC at $O(\alpha_s^4 v^4)$ in Nonrelativistic QCD", Phys. Rev. Lett. **106** (2011) 042002

[6] H. Shao et al., "Yields and polarizations of prompt J/ψ and $\psi(2S)$ production in hadronic collisions", JHEP **05** (2015) 103

[7] ATLAS Collaboration, "Prompt and non-prompt J/ψ elliptic flow in $Pb+Pb$ collisions at $\sqrt{S_{NN}}$=5.02 TeV with the ATLAS detector", Eur. Phys J. C78 (2018) 784

[8] A.M. Poskanzer and S.A. Voloshin, "Methods for analyzing anisotropic flow in relativistic nuclear collisions" , Phys. Rev. C **58** (1998) 1671

[9] ATLAS Collaboration, "Measurement of the production cross section of J/ψ and $\psi(2S)$ mesons at high transverse momentum in pp collisions at $\sqrt{s}$ = 13 TeV with the ATLAS detector, ATLAS-CONF-2019-047

[10] M. Cacciari, S. Frixione and P. Nason, "The p_T spectrum in heavy flavor photoproduction", JHEP **0103** (2001) 006

[11] ATLAS Collaboration, "Measurement of J/ψ production in association with a $W^{\pm}$ boson in pp data at 8 TeV", arXiv:hep-ex 1909.13626

[12] M. Pivk and F. R. Le Diberder, "SPlot: A Statistical tool to unfold data distributions", Nucl. Instrum. Meth. A **555** (2005) 356

[13] P. Cho and A. K. Leibovich, "Color-octet quarkonia production", Phys. Rev. D **53** (1996) 150

[14] P. Cho and A. K. Leibovich, "Color-octet quarkonia production II", Phys. Rev. D **53** (1996) 6203